

# Microwave surface impedance of proximity-coupled superconducting (Nb) / spin-glass (CuMn) bilayers.

L. V. Mercaldo\*, Steven M. Anlage

*Center for Superconductivity Research, Department of Physics, University of Maryland, College Park, MD 20742-4111.*

L. Maritato

*Dipartimento di Fisica, Università degli Studi di Salerno, Baronissi, Salerno I-84081, Italy.*

(November 12, 2017)

## Abstract

The surface impedance of Nb/CuMn (superconducting/spin-glass) bilayers has been measured at 10 *GHz* with the parallel plate resonator technique to obtain information about the exotic behavior of the order parameter in superconducting/magnetic proximity systems. The data strongly differs from the superconducting/normal-metal case, showing the magnetic nature of the CuMn layer, which acts as a weak ferromagnet. The results are described in the framework of two models for the electrodynamics of superconducting/ferromagnetic (S/M) bilayers characterized by a proximity-coupling length scale which is independent of temperature.

PACS: 74.80.Dm, 74.50.+r, 74.25.Nf.

Typeset using REVTeX

---

\*On leave from Dipartimento di Fisica, Università degli Studi di Salerno, Baronissi, Salerno I-84081, Italy.

## I. INTRODUCTION

The issue of the interplay between superconductivity and ferromagnetism has been an intriguing research opportunity for many years [1,2]. Exotic phenomena are predicted for superconducting/ferromagnetic (S/M) coupled layered structures, such as critical temperature oscillations versus the M layer thickness, or spontaneous persistent currents in rings interrupted by an S/M/S junction [3–5]. All of these properties depend on the presence of a spatially dependent phase for the order parameter in the M layer that, for suitable thicknesses, gives rise to a  $\pi$  shift between adjacent superconducting layers. From the experimental point of view, observations of  $T_c$  oscillations, seen as an indirect proof of the  $\pi$  phase, has been reported for Nb/Gd multilayers [6], and Nb/Gd/Nb trilayers [7], and also for Nb/CuMn (superconducting/spin-glass) multilayers [8,9].

Among all the possible S/M proximity coupled layered structures, the superconducting / spin-glass systems are very interesting. Because of the weaker macroscopic magnetism, spin-glass systems offer a wider range of S and M thicknesses in which it is possible to study the influence of magnetism on superconductivity, as compared to the superconducting/ferromagnetic case. Moreover, when using a classical spin-glass such as CuMn, different coupling regimes can be easily selected by changing the Mn concentration, a parameter related to the effective exchange energy  $I$ .

A systematic study of the non-monotonic  $T_c$  vs.  $d_{CuMn}$  behavior in Nb/CuMn multilayers has been previously performed in different coupling regimes, by changing Mn concentration and relative thicknesses [9], showing that an extension of the Radovic *et al.* theory for S/M multilayers [4] to the superconducting/spin-glass case seems very plausible.

More insights into this problem may result from microwave surface impedance measurements, which have provided valuable information about the inhomogeneous superconducting properties of layered systems [10,11]. There are dramatic differences in the electrodynamic properties of superconducting systems with non-uniform order parameter, compared to the homogeneous case. And going backwards, analyzing the electrodynamic properties provides

information about the nature of the induced order parameter in the M layers.

Here we present our results on the surface impedance of Nb/CuMn bilayers with identical Nb base layers and different CuMn layer thicknesses. In Sec. II we describe the sample fabrication and characterization. In Sec. III we illustrate the experimental technique for the surface impedance measurements and we show the data for the bilayers and compare them to the bare Nb case and to previous results on conventional superconductor/normal metal proximity coupled Nb/Cu bilayers [11]. In Sec. IV we present some theoretical background on the S/M proximity effect and introduce two models for the electrodynamics of S/M bilayers, and in Sec. V we apply the models to describe the penetration depth results. In Sec. VI we switch our attention to the surface resistance results, comparing them to the theoretical behavior extracted by applying the models introduced in Sec. IV, and finally in Sec. VII we summarize the results.

## II. SAMPLE FABRICATION AND CHARACTERIZATION

In this work we have focused on Nb/CuMn bilayers with a Mn concentration of 2.7%. We have analyzed seven samples characterized by the same Nb layer thickness ( $d_S = 1500\text{\AA}$ ) and different CuMn layer thicknesses ( $d_M = 30, 60, 90, 120, 150, 180, 240\text{\AA}$ ), where the Nb is the first layer on the substrate. The samples were grown all together in the same deposition run on a 2 inch diameter Si(100) substrate (cut at the end of the process) by a dual source magnetically enhanced dc triode sputtering system with a movable substrate holder. The bilayers were prepared in the same way as the multilayers studied previously [8,9].

After the surface impedance measurements, the top CuMn layer of one pair of samples (the one with  $d_{CuMn}=150\text{\AA}$ ) was removed with a chemical etching, by using a dilute  $HNO_3$  solution, in order to characterize the underlying Nb layer. First of all we have measured the surface impedance of this single Nb layer with the technique described in the next section, obtaining a zero-temperature penetration depth of  $\lambda(0) = 1200\text{\AA}$ . Then we patterned one of the films to perform a resistivity measurement with the standard four-probe technique. The

film has a resistive  $T_c = 7.3K$  [12], a  $10K$  resistivity  $\rho_{Nb}(10K) = 6\mu\Omega \cdot cm$ , and a residual resistivity ratio  $RRR = \rho_{Nb}(300K)/\rho_{Nb}(10K) = 1.9$ . The low  $RRR$  and the high residual resistivity are consistent with both the observed low  $T_c$  and high  $\lambda(0)$  values [13,14], and are probably related to the presence of oxygen in the Nb film. Similar values for all these parameters have been observed, for example, in a Nb-O alloy with a 2% oxygen content [15]. However, the low quality of our Nb does not compromise our work because we compare the behavior of bilayers prepared with identical Nb base layers, so that they differ only in the CuMn layer thickness. The  $T_c$  values for the bilayers are slightly lower than the Nb film (around  $7.1K$ ), as confirmed by ac susceptibility measurements, and this is one indication that the Nb and CuMn layers are proximity-coupled.

We have also prepared a series of CuMn single layer samples with the same thicknesses as those appearing in the bilayers. We have performed Rutherford Backscattering Spectrometry (RBS) measurements on these samples to get the actual Mn concentration and the actual thicknesses. Resistivity measurements have also been performed on some of the thickest samples giving a  $10K$  resistivity value of  $\rho_{CuMn}(10K) = 9\mu\Omega \cdot cm$  for the  $d_{CuMn} = 240\text{\AA}$  case, where this value is expected to be a function of the CuMn layer thickness  $d_{CuMn}$  (it increases upon reducing  $d_{CuMn}$ ), due to finite-size effects [16]. Measurements on CuMn films of three different thicknesses generally agree with this trend. The  $\rho_{CuMn}(T)$  curves for CuMn (figure 1) show an enhancement of the resistivity around  $130K$  often seen for spin-glass materials [17]. Although this enhancement is not related to the spin glass transition, it identifies the two regions where the transport electron - local spin interaction is dominant ( $T > 130K$ ) and where the spin-spin interaction begins to predominate ( $T < 130K$ ). The reduction of the resistivity while decreasing the temperature below the peak value, together with the behavior of other physical properties such as the specific heat, is widely interpreted as an indication of the formation of local correlations and mainly ferromagnetic clusters which gradually reduce the paramagnetic spin disorder scattering [17–19]. This means that even above the spin-glass freezing temperature  $T_f$  the system cannot be described as a simple paramagnet. Low-field ac susceptibility measurements of  $T_f$  in bulk CuMn indicate

$T_f^{bulk} = 18K$  for a 2.7% Mn composition [20], but a lower value is found for thin films because of finite-size effects [16,21,22]. A universal dependence of the normalized freezing temperature  $T_f/T_f^{bulk}$  versus the CuMn layer thickness has been observed while changing the Mn concentration [16,21,22]. Using the curve plotted in ref. [22], we can estimate  $T_f \simeq 14K$  for the thickest sample ( $d_{CuMn} = 240\text{\AA}$ ) and lower values for the other samples until reaching  $T_f \simeq 9K$  for  $d_{CuMn} = 30\text{\AA}$ . Hence for all of our bilayers, the freezing temperature is always larger than the superconducting critical temperature. However, even in the case  $T_f \leq T_c$  no changes are expected in the electrodynamic behavior [23].

### III. SURFACE IMPEDANCE MEASUREMENTS

Surface impedance measurements have been performed on the Nb/CuMn bilayers and on the underlying Nb film at 10 *GHz* by using the parallel plate resonator (PPR) technique [24] with a  $50\mu m$  thick Teflon dielectric spacer.

#### A. Experimental technique

The resonator is formed from two nominally identical thin films clamped face-to-face on a dielectric spacer. The sandwich is placed in a copper chamber in thermal contact with a small copper box in which liquid He can enter from the external dewar through a needle valve. The system (chamber and He box) is enclosed in a vacuum can, where we allow the presence of some He exchange gas ( $P \sim 10\mu mHg$ ), to stabilize the temperature. By pumping on the liquid He in the box the minimum temperature of the sample which can be reached is  $1.7K$ . During the measurement the temperature is gradually increased in discrete steps by means of a computer controlled heater which is in thermal contact with the resonator enclosure.

Excitation of transverse electromagnetic (TEM) modes is accomplished by using two  $50\Omega$  microstrip antennas, whose position can be sensitively varied by micrometers in order to optimize the coupling to the resonator.

For each temperature, we measure, as a function of frequency, the complex transmission coefficient  $S_{21}$  (magnitude and phase) by using a vector network analyzer (some measurements have been done with an HP8510C and others with an HP8722D). The PPR resonant frequency  $f_0$  and quality factor  $Q$  are extracted with an inverse mapping fitting routine in the complex plane [25].

The resistive loss of the superconducting films gives a contribution to the measured  $Q$  of  $Q_{res} = \pi\mu_0 f_0 d / R_S$ , where  $d$  is the spacer thickness and  $R_S$  is the surface resistance of the films. There are, however, additional extrinsic losses, such as the dielectric loss, which is independent of  $d$ , and the radiation loss, which increases linearly with  $d$  [24]. A calibration can be performed by varying the dielectric spacer thickness, so that all these factors can be uniquely determined. However, we found that the PPR modes sometimes lie too close to package resonances, thus changing the  $Q$  values to varying extent depending upon the coupling between the PPR and these parasitic modes [26]. Because of this problem in measuring the intrinsic  $Q$  values, we have only examined the temperature dependence of  $R_S$  and not its absolute value.

## B. Results

Changes in the effective penetration depth have been extracted from the measured resonant frequency by using the expression [11,27]:

$$\Delta\lambda_{eff}(T) = \lambda_{eff}(T) - \lambda_{eff}(T_0) = \frac{d}{2} \left[ \left( \frac{f_0(T_0)}{f_0(T)} \right)^2 - 1 \right]$$

where  $T_0$  is the lowest temperature reached during the measurements (usually  $T_0 \sim 1.7K$ ). In proximity-coupled systems  $\lambda_{eff}$  is an overall screening length which does not correspond to the individual screening lengths of the constituents, because of the non-uniform nature of the superconductivity in the bilayers. Moreover, by using this expression we are not removing the geometric correction due to the finite thickness of the sample, given by the factor  $coth(t/\lambda)$  for a homogeneous superconductor, where  $t$  is the film thickness [28]. In

our case, where  $\lambda(0)$  is the order of  $t$ , this correction is not negligible. Therefore, even in the single-layer Nb film case, we are dealing with an effective penetration depth.

Figure 2 shows the change in the effective penetration depth for the Nb film and the Nb/CuMn (S/M) bilayers, compared to previous results on Nb/Cu (S/N) bilayers [11]. Surprisingly the shape of the  $\Delta\lambda_{eff}(T)$  curves for the S/M bilayers is not very different from the temperature dependence for the Nb, but shows only an enhancement, while a strong linear-in-temperature character was evident in  $\Delta\lambda_{eff}(T)$  for Nb/Cu. Moreover there is no systematic dependence of  $\Delta\lambda_{eff}(T)$  on the CuMn layer thickness, in striking contrast to the case of Nb/Cu bilayers, where a strong dependence of  $\Delta\lambda_{eff}(T)$  on the normal layer thickness has been observed. Results similar to Nb/Cu have also been obtained for Nb/Al bilayers [10].

Figure 3 shows the temperature dependence of the effective surface resistance, minus the residual value at  $T_0$ , for the Nb film and the bilayers. Again the Nb/Cu data [11], corrected for extrinsic losses, have been plotted for comparison. The data have been extracted from the measured quality factor  $Q$  by using the relation  $R_S = \pi\mu_0 f_0 d/Q$  [24], neglecting dielectric and radiation losses [11], and then the low temperature residual resistance  $R_{S0} = R_S(T_0)$  has been subtracted. From this point of view it is interesting to observe that as for  $\Delta\lambda_{eff}(T)$ , also the  $R_S(T)$  behavior is similar to the BCS behavior (Nb data are shown as inverted triangles on fig. 3), and again there is no systematic variation with  $d_{CuMn}$ . These results are in striking contrast to the results on Nb/Cu, where also a low-temperature downturn of  $R_S(T)$  was observed that is missing here. Note, also, that the Nb/CuMn data fall into two groups: one composed of the thin CuMn layer films, which are very close to the pure Nb film, and a second group composed of thicker films (together with the 90Å CuMn sample) which show enhanced  $R_S - R_{S0}$ .

In figures 2 and 3 the changes in the effective penetration depth and the effective surface resistance for the Nb underlayer are reported together with the results for the bilayers. In figure 4 these quantities (solid symbols) are compared to the corresponding intrinsic one (open symbols), obtained by performing a finite thickness correction, as given by Klein *et.*

*al.* [28], in conjunction with the BCS-Mühlschlegel [29] fit. The solid line in the figure is the BCS-Mühlschlegel fit to the intrinsic data, which gives  $T_c = 7.7K$  and  $\lambda(0) = 1200\text{\AA}$ . In both cases the effective quantity is strongly enhanced compared to the intrinsic one, since  $\lambda(0) \sim t$ . Concerning  $R_S$ , again we are neglecting the dielectric and radiation losses, which partly explains the high residual value shown in figure 4.

#### IV. MODELS FOR THE S/M BILAYER ELECTRODYNAMICS

To understand the origin of the different behavior in S/M and S/N proximity systems we need to analyze the order parameter that describes the extent of the proximity coupling, given by the pair potential  $\Delta(\vec{r}) = V(\vec{r}) \langle \psi_\uparrow(\vec{r}) \psi_\downarrow(\vec{r}) \rangle$ . Here  $V(\vec{r})$  is the electron-electron attractive interaction responsible for superconductivity and  $\langle \psi_\uparrow(\vec{r}) \psi_\downarrow(\vec{r}) \rangle$  is the probability amplitude to find a Cooper pair in the position  $\vec{r}$ . In the usual picture of the single frequency approximation in S/N bilayers  $\Delta(\vec{r})$  decreases from its bulk value in the vicinity of the S/N interface in the S material, while a non-zero order parameter is induced on the N side, decaying exponentially as the free surface is approached [30]. For the penetration depth, the widely accepted approximation [31]  $\lambda(\vec{r}) \propto \frac{1}{\Delta(\vec{r})}$  gives it an exponential dependence in the N (non-magnetic) layer.

The magnetic case is more complicated and a new treatment is required. Based on our previous results for  $T_c$  vs.  $d_{CuMn}$  oscillations [8,9], we want to apply the same Radovic *et al.* theory [4] to propose a spatial dependence for  $\lambda(\vec{r})$ . Radovic *et al.* show that in a magnetic metal, where  $\Delta_M = 0$  because the BCS coupling is identically zero, the Green function  $F_M$  describing the condensate of pairs is non-zero, due to the proximity of S. Its real part (and imaginary part) exhibits an oscillatory behavior damped by the exponential decay usual in S/N systems. Moreover, in this theory, developed in the dirty limit, the characteristic penetration length of the Cooper pairs in M, defined as  $\xi_M = \sqrt{4\hbar D_M / |I|}$ , depends on the diffusion coefficient  $D_M = \frac{1}{3} v_F l_M$  and on the exchange energy  $I$  but is temperature independent and typically much smaller than the corresponding length in a normal metal



with  $D_N = D_M$ , that is given by  $\xi_N = \sqrt{\hbar D_N / 2\pi k_B T}$ . Here  $v_F$  is the Fermi velocity and  $l_M$  is the mean free path of quasiparticles in the M layer. A temperature independent and small penetration of Cooper pairs in M was already predicted by the combination of the de Gennes-Werthamer theory for S/N proximity effect [30,32] and the Abrikosov and Gor'kov analysis for the role of paramagnetic impurities in a superconductor [33], as shown in ref. [34].

Even if  $\Delta_M = 0$ , due to the proximity effect the Cooper pair probability amplitude  $\langle \psi_\uparrow(\vec{r}) \psi_\downarrow(\vec{r}) \rangle_M$  is non-zero and has the same oscillating and damped behavior of  $F_M$ . If we call  $x$  the axis perpendicular to the interface and we identify the interface position as  $x = 0$ , so that the M layer extends from  $x = 0$  to  $x = -d_M$  while the S layer extends from  $x = 0$  to  $x = d_S$  (see inset of fig. 5), in the bilayer case this amplitude can be written as:

$$\langle \psi_\uparrow(x) \psi_\downarrow(x) \rangle_M \propto \exp(k_M x) \quad -d_M \leq x \leq 0$$

with  $k_M$  complex [36], which means that the Cooper pairs acquire a spatially dependent phase in the magnetic layer, while their density, which is proportional to  $|\langle \psi_\uparrow(x) \psi_\downarrow(x) \rangle_M|^2$ , decays exponentially. In this picture, assuming now  $\lambda_M(x) \sim |\langle \psi_\uparrow(x) \psi_\downarrow(x) \rangle_M|^{-1}$  (a local inverse proportionality between  $\lambda_M^2(x)$  and the Cooper pair probability density) we have again an exponential dependence for  $\lambda_M$ , but with a characteristic length  $(\text{Re } k_M)^{-1} \sim \xi_M$  that is temperature-independent and smaller than that observed in the S/N case:

$$\lambda_M(x, T) = \lambda_M(0, T) \exp[-(\text{Re } k_M)x] \quad -d_M \leq x \leq 0$$

All the temperature dependence of  $\lambda_M$  enters in the coefficient  $\lambda_M(0, T)$  for which the BCS temperature dependence can be assumed.

Therefore, on the basis of this simple theory, we conclude that the oscillating behavior of the induced pair amplitude cannot be detected in our experiment, since we are only sensitive to its modulus. However we can check to see if our experimental results are consistent with a picture in which  $\lambda_M(x, T)$  has a strong exponential behavior with a characteristic length which is not dependent on temperature. This also means that we can use existing models for the electrodynamics of S/N bilayer systems [27,35] with minor changes.

We shall now summarize the two leading models of the electrodynamics of S/N bilayers. In the first model (Model I) we assume that the non-superconducting layer is active in screening the applied magnetic field and, on the other side, the S layer is unaffected by the presence of the non-superconducting layer, so that  $\lambda_S$  is uniform across all the S layer and its temperature dependence is that given by the BCS theory [29]. In the M layer we take  $\lambda_M(x, T) = \lambda_M(0, T) \exp(kx)$  (see inset of fig. 5). Because of the small value we expect for  $k^{-1}$  in the magnetic case, which means almost no screening of the magnetic field by the M layers, we also consider a second model (Model II) in which the M layer does no screening at all ( $\lambda_M(x) \rightarrow \infty$ ) [37], while the superconducting properties of the S layer are suppressed near the interface. Following de Gennes [38], in Model II we assume in particular that the order parameter in S decreases, upon approaching the interface, as  $\Delta_S(x, T) = \Delta_0 \tanh \frac{x-x_0}{\sqrt{2}\xi_S(T)}$  ( $x > 0$ ), which means that the penetration depth is enhanced following the dependence  $\lambda_S(x, T) = \lambda_{S0}(T) \coth \frac{x-x_0}{\sqrt{2}\xi_S(T)}$  ( $x > 0$ ), where  $\lambda_{S0}(T)$  is the bulk penetration depth,  $\xi_S$  is the superconducting coherence length,  $x_0 = -\frac{\xi_S}{\sqrt{2}} \ln \left( \frac{\sqrt{2}b}{\xi_S} + \sqrt{\frac{2b^2}{\xi_S^2} + 1} \right)$  and  $b$  is the extrapolation length, proportional to the coherence length of the adjacent non-superconducting layer (see inset of fig. 5).

We consider Models I and II to be two extreme cases in which the altered screening in either the M or S layer dominates the proximity screening. Actually in general the real process involves both kinds of physics, although we expect it to be dominated by one or the other. Moreover, in both of the models we are not explicitly taking into account the transparency of the S/M interface for Cooper pairs, that is an important parameter in these systems [40]; however, the behavior at the interface is hidden in the parameter values.

The details about the calculations of the tangential magnetic field  $H(x)$ , the supercurrent density  $J_S(x)$  and the effective penetration depth  $\lambda_{eff}$  may be found in refs. [27,35]. These expressions have been used, with appropriate modifications for the S/M case, in the discussion below.

## V. COMPARISON OF DATA AND MODELS

We found previously that in the S/N bilayer case, Model II could not describe the  $\Delta\lambda_{eff}(T)$  data, because the theoretical behavior is not very different from a BCS s-wave temperature dependence [27,35]. Model I, instead, was found to describe the  $\Delta\lambda_{eff}(T)$  data very well [10,11]. Here we report the analysis of the Nb/CuMn data with both of the models introduced in the previous section. Actually in the S/M case we do not expect much screening in the M layer, in which case Model II may be more appropriate. However, in principle we do not know *a priori* if CuMn is really acting as a ferromagnet in the screening process. And through Model I we can do a more direct comparison with the S/N case, in particular by looking at the proximity length scale  $k^{-1}$  value and its temperature dependence.

### A. Model I

In the S/N case, it was crucial to use a proximity length scale  $k^{-1}$  which was temperature dependent to get a good fit to the data. In this way in the low  $T$  region  $\lambda_{eff}(T)$  is a strongly increasing function of temperature and the shape of the curves depends on  $d_N$ . In particular,  $k^{-1}(T) \sim T^{-1/2}$  was found for Nb/Al [10] and  $k^{-1}(T) \sim T^{-2}$  for Nb/Cu [11]. In contrast, with  $k$  independent of  $T$ ,  $\lambda_{eff}(T)$  is flat at low  $T$  (below  $T/T_c \simeq 1/4$ , with the  $k^{-1}$  value used here, that is reported below) independent of  $d_M$ , and  $\Delta\lambda_{eff}(T)$  is essentially zero for all the non-superconducting layer thicknesses. At higher temperatures the curves increase together in a manner which is independent of  $d_M$ . This is just the temperature behavior we have observed in the S/M case. Thus the Nb/CuMn experimental results are qualitatively consistent with a  $\xi_M$  which is independent of temperature.

The solid curve in figure 5, which describes well all the  $\Delta\lambda_{eff}(T)$  data on the Nb/CuMn bilayers, has been obtained using reasonable values for all the parameters, as shown in Table 1. However, even though the agreement with the model looks good, Model I is not really appropriate to describe S/M bilayers, where the proximity length scale  $k^{-1}$  is very short

( $k^{-1} \ll \lambda_M(0,0)$ ) [31]. Indeed, in Model I the assumption  $\lambda_M(x) \sim |\langle \psi_\uparrow(x) \psi_\downarrow(x) \rangle_M|^{-1}$  forces the screening length to be regulated by the proximity length scale  $k^{-1}$ . In the S/M case this implies huge current densities in a narrow region ( $\sim \xi_M$ ) near the interface, while there is a small screening activity in the S layer, which is not a physically reasonable scenario.

In summary, using Model I, we found a temperature independent proximity effect correlation length (as expected on the basis of the Radovic *et al.* picture for S/M multilayers [4]), and we learned that almost all the screening activity happens in the superconducting layer. These results confirm that the CuMn layer is acting as a ferromagnet in the screening process. However, the screening activity picture given by Model I is unphysical. The main reason is that the spatial variation of  $\lambda_S$  in the superconductor is not taken into account and this can be a good approximation in the S/N case but not in the S/M case. These problems are addressed in Model II.

## B. Model II

In Model II we are assuming that the penetration depth is infinitely large in M and a decreasing function of  $x$  in S going from the interface ( $x = 0$ ) to the opposite edge ( $x = d_S$ ), and the extrapolation length  $b \sim \xi_M$  dictates the behavior at the interface (see inset of figure 5). As with  $k^{-1}$  in Model I, this parameter ( $b$ ) is temperature independent in the S/M case. As in Model I we again do not obtain any dependence of  $\Delta\lambda_{eff}(T)$  on the M layer thickness.

The parameters in Model II are the Nb critical temperature  $T_c$ , the extrapolation length  $b$ , the zero-temperature superconducting coherence length  $\xi_S(0)$ , and the zero temperature penetration depth  $\lambda_{S0}$  far from the interface. In Model II only parameters characteristic of the S layer appear, except for  $b$ , which is the only parameter directly dependent upon the nature of the non superconducting layer. We have used  $T_c = 7.7K$  and  $\lambda_{S0} = 1200\text{\AA}$ , as obtained from the analysis of the single layer Nb film,  $b = \xi_M = 19\text{\AA}$ , which comes from the previous work on the  $T_c$  oscillations vs.  $d_{CuMn}$  multilayers [9] (however, a value between 0 and 100  $\text{\AA}$  still describes the data well), and  $\xi_S(0) = 150\text{\AA}$  (Table 1). The  $\xi_S(0)$  value has

been chosen as close as possible to the dirty limit coherence length  $\xi_S = \sqrt{\hbar D_S / 2\pi k_B T_c}$  [4], with  $D_S = v_F l_S / 3$  the diffusion coefficient in S and  $l_S$  the mean-free path in S. From the measured low temperature resistivity value we get  $l_S = 63\text{\AA}$ , which gives  $\xi_S = 93\text{\AA}$ . The curve for the Model II prediction of  $\Delta\lambda_{eff}(T)$  is shown in figure 5 (dashed line). This model does an excellent job of fitting the data, and moreover addresses the problems encountered in Model I. In particular it takes into account the suppression of the superconducting properties in the S layer at the interface, which is not negligible in the S/M case. Indeed, due to the very small  $b$  value ( $b \sim 0$  to  $100\text{\AA}$ ), we observed here  $\Delta_S(x=0)/\Delta_{S,bulk} \sim 0$  to  $0.4$  for  $T \rightarrow 0$  for all the Nb/CuMn bilayers (in particular for  $b = 19\text{\AA}$  this ratio is  $\sim 0.09$ ), where this ratio is even smaller at higher temperatures.

In conclusion Model II captures the essence of the electrodynamics of S/M bilayers (screening dominated by the S layer which has a strongly suppressed order parameter near the interface) and the fit is done with independently determined parameters.

## VI. SURFACE RESISTANCE IN MODEL II

In this section we want to extend Model II to describe also the surface resistance data. The surface resistance  $R_S$  can be calculated by using the relation [10,27]:

$$R_S(T) = \frac{\mu_0^2}{H_0^2} \int_{-d_M}^{d_S} \frac{\sigma_1(x, T)}{\sigma_1^2(x, T) + \sigma_2^2(x, T)} J^2(x, T) dx$$

where  $\sigma_1(x, T)$  and  $\sigma_2(x, T)$  are the real and imaginary parts of the local conductivity,  $H_0$  is the applied field and  $J$  is the total current density. Again, we have to remember that we are dealing with an effective surface resistance, not only because of the non-uniformity of the magnetic screening, but also because of the finite sample thickness.

To obtain an estimate for  $R_S(T)$  in the bilayers, in a first approximation we have used the current density calculated before with Model II to get  $\lambda_{eff}$ , even though it was derived neglecting the normal currents. As for the local conductivity, we have taken  $\sigma_2(x, T) = [\omega\mu_0\lambda^2(x, T)]^{-1}$ , where we have used the Model II spatial dependence of  $\lambda(x, T)$ , while for

$\sigma_1(x, T)$  we have used a generalized Mattis-Bardeen [39] expression in which the local BCS gap  $\Delta_S(x, T)$  used in model II (the expression is reported in Sec. IV) replaces the spatially uniform one found in homogeneous superconductors [27].

Model II only calculates the contribution to  $R_s$  coming from S; the contribution from M is only an additive constant term. Therefore we obtain for  $R_S(T)$  something that goes to zero at low temperature, so to compare with the experimental behavior, we subtracted the lowest temperature residual resistance  $R_{S0} = R_S(T_0)$  from the data (as in figures 3 and 6).

The theoretical curves in figure 6 have been obtained with the same parameter values used for the  $\Delta\lambda_{eff}(T)$  analysis (i.e.  $T_c$ ,  $\lambda_{S0}$ ,  $\xi_S(0)$ ,  $b$ ). The gap value has been chosen equal to the BCS value  $\Delta_0 = 1.76k_B T_c$ , and a complete freedom has been left for the low temperature normal state conductivity  $\sigma_S$  in S. The  $\sigma_S$  values found with the fit procedure are only slightly lower than that measured. Table 1 summarizes the parameter values, and the fits are shown as dashed lines in figure 6.

In figure 6 we also show fits obtained using Model I (solid lines). In this case, to evaluate the generalized Mattis-Bardeen  $\sigma_1(x, T)$  in M, for simplicity we did not take into account any effect due to the spatial dependence of the phase of the order parameter in M and we used a decaying real exponential dependence for  $\Delta_M(x, T)$ , as for the S/N bilayer case [41]. With Model I unreasonably large  $\sigma_S$  values had to be used to get close to the data (the fit parameters are reported in Table 1).

In summary, the theoretical treatment of the surface resistance with Model II gives a satisfactory understanding of the  $R_S(T)$  behavior using the same parameter values as for the analysis of the penetration depth temperature and  $d_{CuMn}$  dependence data.

## VII. CONCLUSIONS

In conclusion, microwave surface impedance measurements have been performed on Nb/CuMn superconducting/spin-glass proximity coupled bilayers. Both  $\Delta\lambda_{eff}(T)$  and  $R_S(T)$  results are very different from the Nb/Cu case, showing that the superconduct-

ing properties of the Nb layer are strongly suppressed near the interface and the CuMn layer does not participate too much in the screening of the applied rf magnetic field. These are exactly the results we expect for a proximity effect between a superconductor and a ferromagnet. Therefore they confirm that the CuMn layer is acting as a weak ferromagnet. Moreover, these measurements can be described with a proximity effect correlation length which does not depend on temperature, consistent with previous data on  $T_c$  oscillations vs. CuMn layer thickness, and the Radovic *et al.* theoretical picture for S/M systems [4]. This work sets also the stage to investigate more directly the presence of a  $\pi$ -phase shift in superconducting/ferromagnetic (spin-glass) layered structures with the Nb/CuMn system.

### VIII. ACKNOWLEDGMENTS

We thank M. S. Pambianchi for his contributions in the design of the probe and in the development of model calculations for the S/N case, P. Fournier for assistance with the resistivity measurements, and R. P. Sharma and S. Choopun who performed the RBS analysis.

This work is supported by the National Science Foundation through grant number DMR-96-24021.

## REFERENCES

- [1] K. Maki, in *Superconductivity*, edited by R. D. Parks (Dekker, New York, 1969), p.1035 and references therein.
- [2] A. J. Millis and H. Monien, Phys. Rev. Lett. **70**, 2810 (1993); S. Katano, T. Matsumoto, A. Matsushita, T. Hatano, and S. Funahashi, Phys. Rev. B **41**, 2009 (1990).
- [3] L. N. Bulaevskii, V. V. Kuzii, and A. A. Sobyenin, JETP Lett. **25**, 290 (1977); A. I. Buzdin, L. N. Bulaevskii, S. V. Panyukov, JETP Lett. **35**, 178 (1982); A. V. Andreev, A. I. Buzdin, and R. M. Ozgud, JETP Lett. **52**, 55 (1990); A. I. Buzdin and M. Y. Kupriyanov, JETP Lett. **52**, 487 (1990); A. I. Buzdin and M. Y. Kupriyanov, JETP Lett. **53**, 321 (1991); A. I. Buzdin, B. Bujicic, and M. Y. Kupriyanov, Sov. Phys. JETP **74**, 124 (1992).
- [4] Z. Radovic, M. Ledvij, L. Dobrosavljevic-Grujic, A. I. Buzdin, and J. R. Clem, Phys. Rev. B **44**, 759 (1991).
- [5] E. A. Demler, G. B. Arnold, and M. R. Beasley, Phys. Rev. B **55**, 15174 (1997).
- [6] J. S. Jiang, D. Davidovic, D. H. Reich, and C. L. Chien, Phys. Rev. Lett. **74**, 314 (1995).
- [7] J. S. Jiang, D. Davidovic, D. H. Reich, and C. L. Chien, Phys. Rev. B **54**, 6119 (1996).
- [8] L. V. Mercaldo, C. Attanasio, C. Coccorese, L. Maritato, S. L. Prischepa, and M. Salvato, Phys. Rev. B **53**, 14040 (1996).
- [9] C. Attanasio, C. Coccorese, L. V. Mercaldo, S. L. Prischepa, M. Salvato, and L. Maritato, Phys. Rev. B **57**, 14411 (1998).
- [10] M. S. Pambianchi, S. N. Mao, S. M. Anlage, Phys. Rev. B **52**, 4477 (1995).
- [11] M. S. Pambianchi, L. Chen, and S. M. Anlage, Phys. Rev. B **54**, 3508 (1996).
- [12] The value reported in the text for  $T_c$  is the zero-resistance transition temperature, while



the onset is at 7.5K and the fit of the penetration depth data to the BCS theory gives  $T_c = 7.7K$ .

- [13] C. Camerlingo, P. Scardi, C. Tosello, and R. Vaglio, Phys. Rev. B **31**, 3121 (1985); L. R. Testardi and L. F. Mattheiss, Phys. Rev. Lett. **41**, 1612 (1978).
- [14] A. Andreone, A. Cassinese, M. Iavarone, R. Vaglio, I. I. Kulik and V. Palmieri, Phys. Rev. B **52**, 4473 (1995).
- [15] C. C. Koch, J. O. Scarbrough, and D. M. Kroeger, Phys. Rev. B **9**, 888 (1974); J. Halbritter, Appl. Phys. A **43**, 1 (1987).
- [16] G. G. Kenning, J. M. Slaughter, and J. A. Cowen, Phys. Rev. Lett. **59**, 2596 (1987).
- [17] J. A. Mydosh, Journal of Magnetism and Magnetic Materials **7**, 237 (1978).
- [18] I. A. Campbell, Phys. Rev. Lett. **47**, 473 (1981); I. A. Campbell, P. J. Ford, and A. Hamzic, Phys. Rev. B **26**, 5195 (1982).
- [19] J. A. Mydosh, in *Heidelberg Colloquium on Spin-glasses*, Proceedings, Heidelberg 1983, edited by J. L. Hemmen and I. Morgenstern (Springer Verlag, 1983), p.38.
- [20] P. J. Ford and J. A. Mydosh, Phys. Rev. B **14**, 2057 (1976).
- [21] G. G. Kenning, J. Bass, W. P. Pratt, Jr., D. Leslie-Pelecky, L. Hoines, W. Leach, M. L. Wilson, R. Stubi, and J. A. Cowen, Phys. Rev. B **42**, 2393 (1990).
- [22] L. Hoines, R. Stubi, R. Loloee, J. W. Cowen, and J. Bass, Phys. Rev. Lett. **66**, 1224 (1991).
- [23] Sharp features are observed at the freezing temperature in ac susceptibility, magnetization, anomalous Hall effect, Mössbauer effect,  $\mu^+$  depolarization, while in specific heat, resistivity, thermopower and electron spin resonance, only broad changes over a wide temperature range have been observed [17].

- [24] R. C. Taber, Rev. Sci. Instrum. **61**, 2200 (1990); M. S. Pambianchi, S. M. Anlage, E. S. Hellman, E. H. Hartford, Jr., M. Bruns, and S. Y. Lee, Appl. Phys. Lett. **64**, 244 (1994).
- [25] P. Petersan and S. M. Anlage, J. Appl. Phys. **84**, 3392 (1998), and xxx@lanl.gov/condmat/9805365.
- [26] F. Gao, M. V. Klein, J. Kruse, and M. Feng, IEEE Trans. Microwave Theory Tech. **44**, 944 (1996).
- [27] M. S. Pambianchi, Ph. D. thesis, University of Maryland, 1995.
- [28] N. Klein, H. Chaloupka, g. Müller, S. Orbach, H. Piel, B. Roas, L. Schultz, U. Klein, and M. Peiniger, J. Appl. Phys. **67**, 6940 (1990).
- [29] B. Mühlshlegel, Z. Physik **155**, 313 (1959).
- [30] P. G. de Gennes and E. Guyon, Phys. Lett. **3**, 168, (1963).
- [31] G. Deutscher and P. G. de Gennes, in *Superconductivity*, edited by R. D. Parks (Dekker, New York, 1969), p. 1005; G. Deutscher, J. P. Hurault, and P. A. van Dalen, J. Phys. Chem. Solids **30**, 509 (1969).
- [32] N. R. Werthamer, Phys. Rev. **132**, 2440 (1963).
- [33] A. Abrikosov and L. P. Gor'kov, Sov. Phys. JETP **12**, 1243 (1961).
- [34] J. J. Hauser, H. C. Theuerer and N. R. Werthamer, Phys. Rev. **142**, 118 (1966).
- [35] M. S. Pambianchi, J. Mao, and S. M. Anlage, Phys. Rev. B **50**, 13659 (1994).
- [36] The general expression for  $k_M$  is  $k_M^2 = 2 \frac{\hbar\omega + iI}{\hbar D_M} \text{sgn}\omega$ , where  $\omega = \frac{\pi k_B T}{\hbar} (2n + 1)$  are the Matsubara frequencies, but the expression  $k_M^{-1} = (1 - i \text{sgn}\omega \text{sgn}I) \sqrt{\frac{\hbar D_M}{4I}}$ , valid in the limit  $I \gg k_B T_{cs}$ , is generally used [4].
- [37] To be more precise, in Model II we should assume that  $\lambda_M$  approaches the normal metal

skin depth  $\delta$ . However, the CuMn layer thickness is much smaller than  $\delta$  and there is no screening.

[38] P. G. de Gennes, *Superconductivity of Metals and Alloys* (Addison-Wesley, Radwood City, 1989), p.233; P. G. de Gennes and J. Matricon, *Solid State Commun.* **3**, 151 (1965).

[39] D. C. Mattis and J. Bardeen, *Phys. Rev* **111**, 412 (1958).

[40] J. Aarts, J. M. E. Geers, E. Brück, A. A. Golubov and R. Coehoorn, *Phys. Rev. B* **56**, 2779 (1997).

[41] As pointed out in Sec. IV,  $\Delta_M = 0$  in M layers, therefore, to be precise, we should do a treatment in terms of the Green function  $F_M$  or of the pair amplitude  $\langle \psi_\uparrow \psi_\downarrow \rangle_M$ .

## FIGURES

FIG. 1. Resistivity versus temperature curve for the 150Å thick CuMn sample. Similar behavior has been observed for CuMn samples of different thickness.

FIG. 2. Changes in the effective penetration depth,  $\Delta\lambda_{eff}(T)$ , with respect to temperature for the bare Nb film and the Nb/CuMn bilayers (open symbols and left axis) compared to the Nb/Cu data (solid symbols and right axis). The Nb/Cu data are shown with an arbitrary offset in the vertical direction for clarity. The data are plotted versus the normalized temperature  $T/T_c$ , where the critical temperature used here for our data (6.6K) is lower than the resistive value measured for the Nb underlayer (7.3K). The Cu layer thicknesses in Å are reported in the legend, while the CuMn layer thicknesses appear in figure 6 next to the symbols used in the figure.

FIG. 3. Effective surface resistance ( $R_S$ ) minus the residual value at the minimum temperature ( $R_{S0}$ ) vs. the normalized temperature  $T/T_c$  for the Nb film (inverted triangles) and the Nb/CuMn bilayers, together with the  $R_S(T)$  data for the Nb/Cu case corrected for extrinsic losses. We have adopted the same symbols as in figure 2. For the CuMn layer thicknesses refer to fig. 6 and for the Cu layer thicknesses to fig. 2.

FIG. 4. Effective (solid symbols) and intrinsic (open symbols) changes in the penetration depth (circles and left axis) and surface resistance (squares and right axis) of the Nb undelayer. The effective quantities have been altered by geometrical effects due to the finite thickness of the films. The solid line in the figure is the fit to the BCS theory.

FIG. 5. Comparison between the experimental changes in the effective penetration depth for the Nb/CuMn bilayers and the theoretical curves obtained with the models described in the text. The CuMn layer thicknesses in Å appear in fig. 6 (we are adopting the same symbols). Inset: S/M bilayer geometry with the magnetic-field boundary conditions and the schematic variation of order parameter and penetration depth in Model I and Model II (in Model II the M layer does not screening at all, i. e.  $\lambda_M(x) \rightarrow \infty$ ).

FIG. 6. Surface resistance minus the residual value at the minimum temperature for all the bilayers together with the theoretical curves obtained with the models presented in the text. The theoretical curves describing the lower  $R_S - R_{S0}$  data group are characterized by a lower Nb 10K conductivity value ( $\sigma_S$ ). The legend shows the CuMn layer thicknesses in Å.

Table 1. Summary of the values of all the parameters appearing in this work. The fitting parameter values obtained in the  $\Delta\lambda_{eff}(T)$  and  $R_S(T)$  analyses in both Model I and Model II are compared with the corresponding measured or otherwise determined values. In particular  $T_c$ ,  $\sigma_S$  and  $\sigma_M$  have been resistively measured,  $\lambda_S(0)$  was determined by fitting the frequency shift data for the bare Nb to the BCS theory (in parentheses we show also the  $T_c$  obtained with this procedure),  $\xi_S(0)$  is the predicted dirty limit value with the BCS-determined  $T_c$ , and for  $k^{-1}$  and  $b$  we report here the  $\xi_M$  value obtained in the previous work on the  $T_c$  oscillations in Nb/CuMn multilayers with the same Mn concentration [9].

parameter	'measured'	from $\Delta\lambda_{eff}(T)$ fit		from $R_S(T)$ fit	
		Model I	Model II	Model I	Model II
$T_c (K)$	7.3 (7.7)	7.7	7.7	7.7	7.7
$k^{-1} (\text{\AA})$	$\sim \xi_M = 19$	19	-	19	-
$b (\text{\AA})$	$\sim \xi_M = 19$	-	0 to 100	-	0 to 100
$\xi_S(0) (\text{\AA})$	93	-	150	-	150
$\lambda_S(0) (\text{\AA})$	1200	1200	1200	1200	1200
$\lambda_M(0,0) (\text{\AA})$	-	$\sim 120$	-	$\sim 120$	-
$\sigma_S (10^7/\Omega \cdot m)$	1.7	-	-	5 to 10	.7 to 1.2
$\sigma_M (10^7/\Omega \cdot m)$	1	-	-	1	-

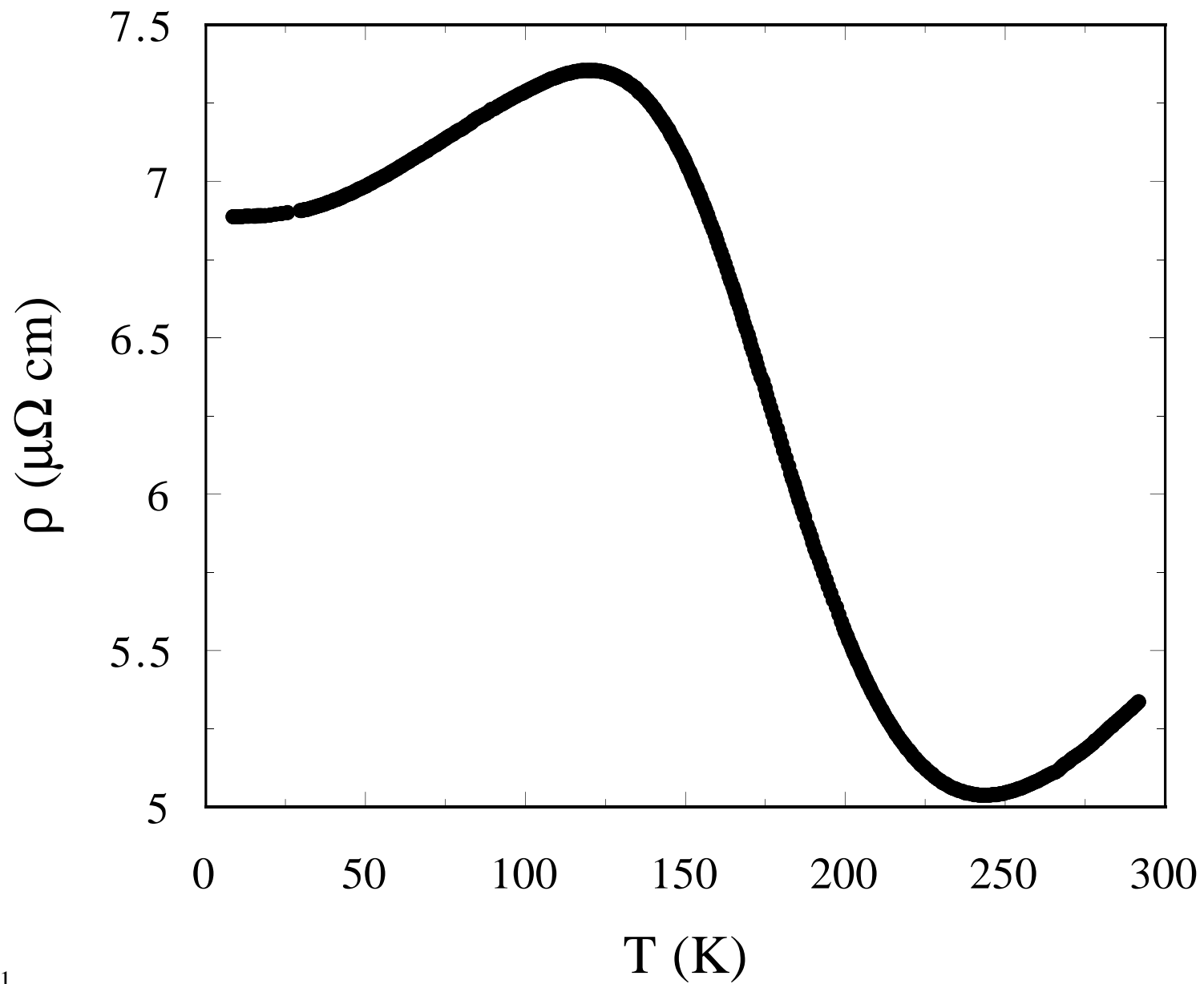


Fig. 1  
L. V. Mercaldo et al.

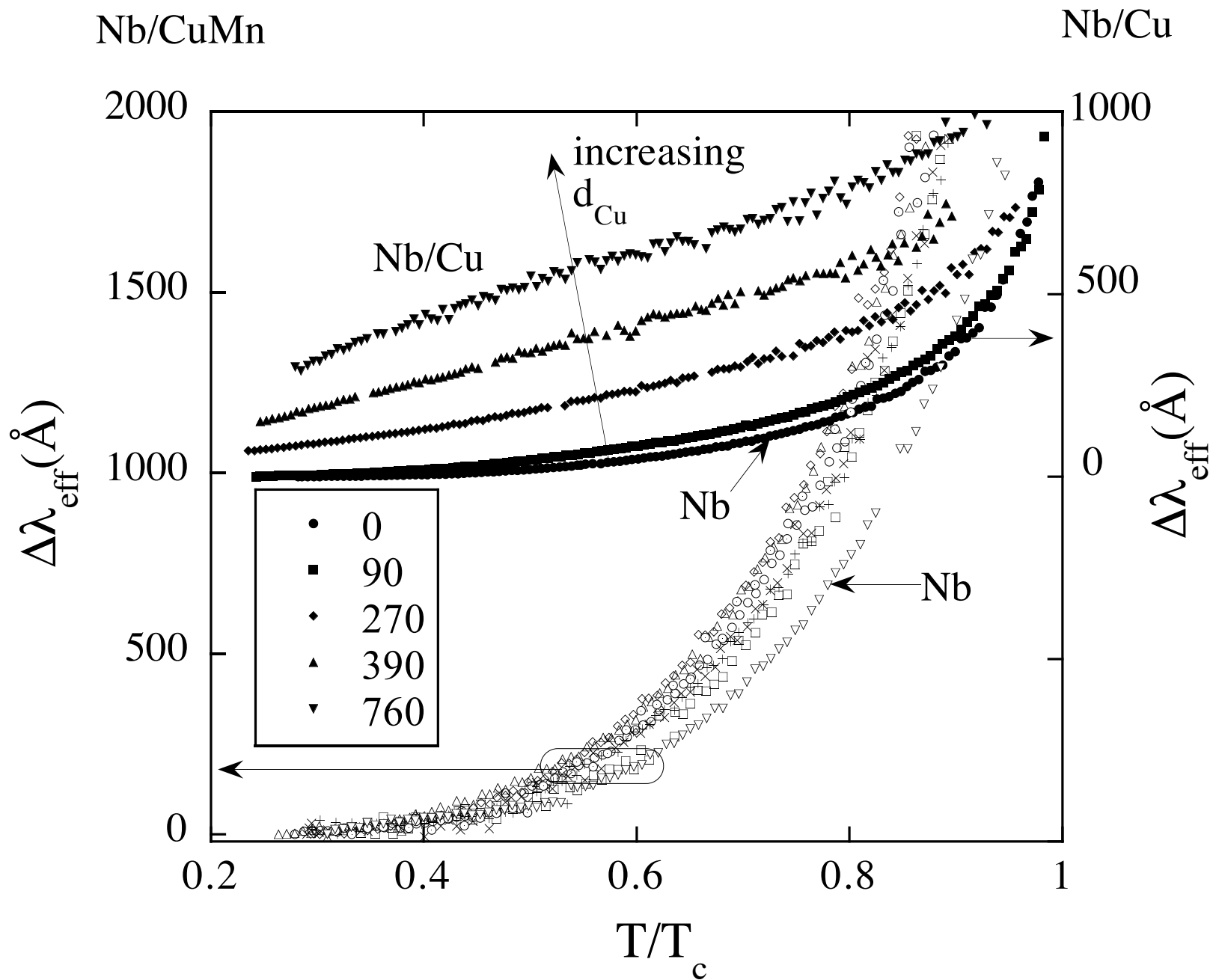


Fig. 2  
 L. V. Mercaldo et al.



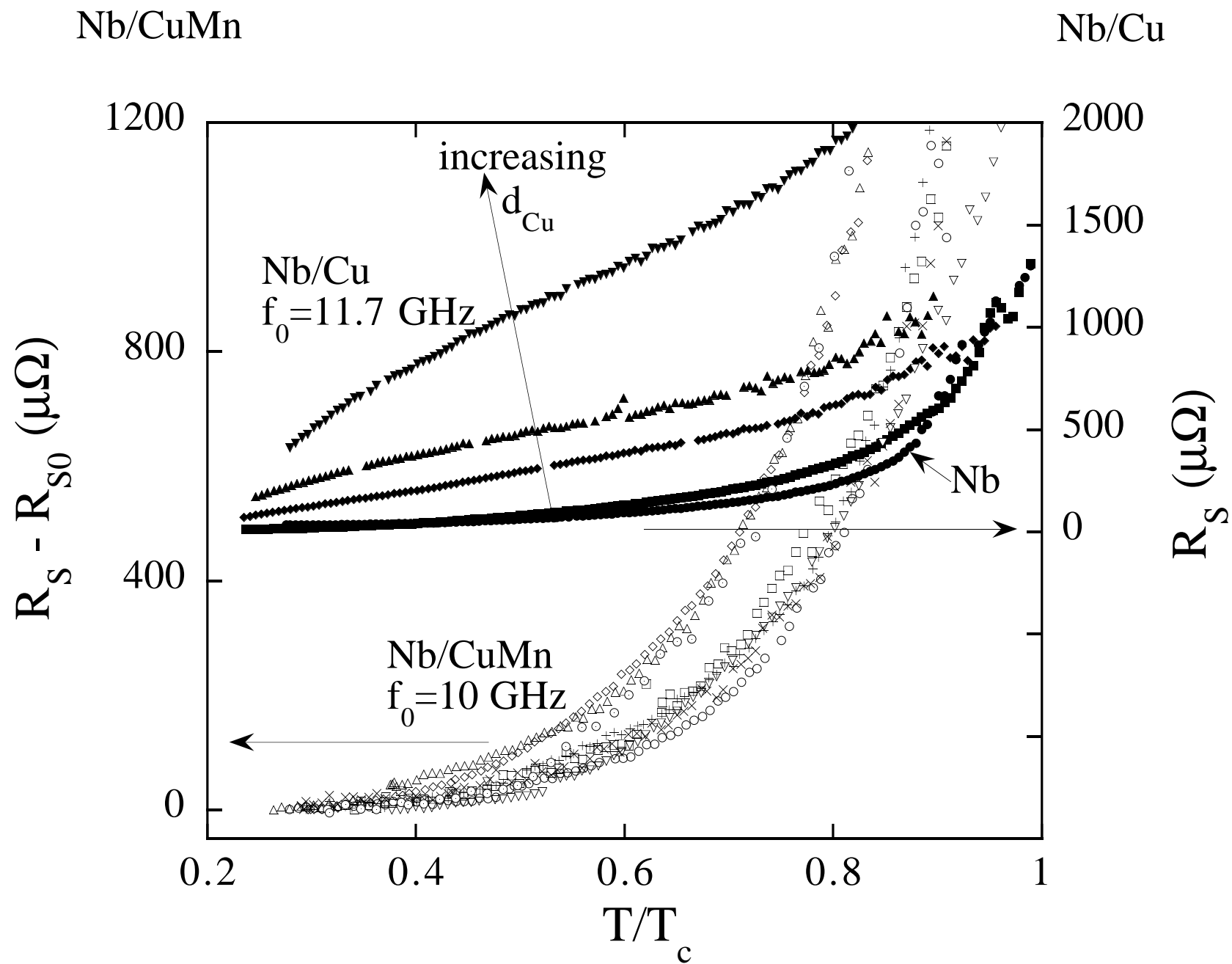


Fig. 3  
 L. V. Mercaldo et al.

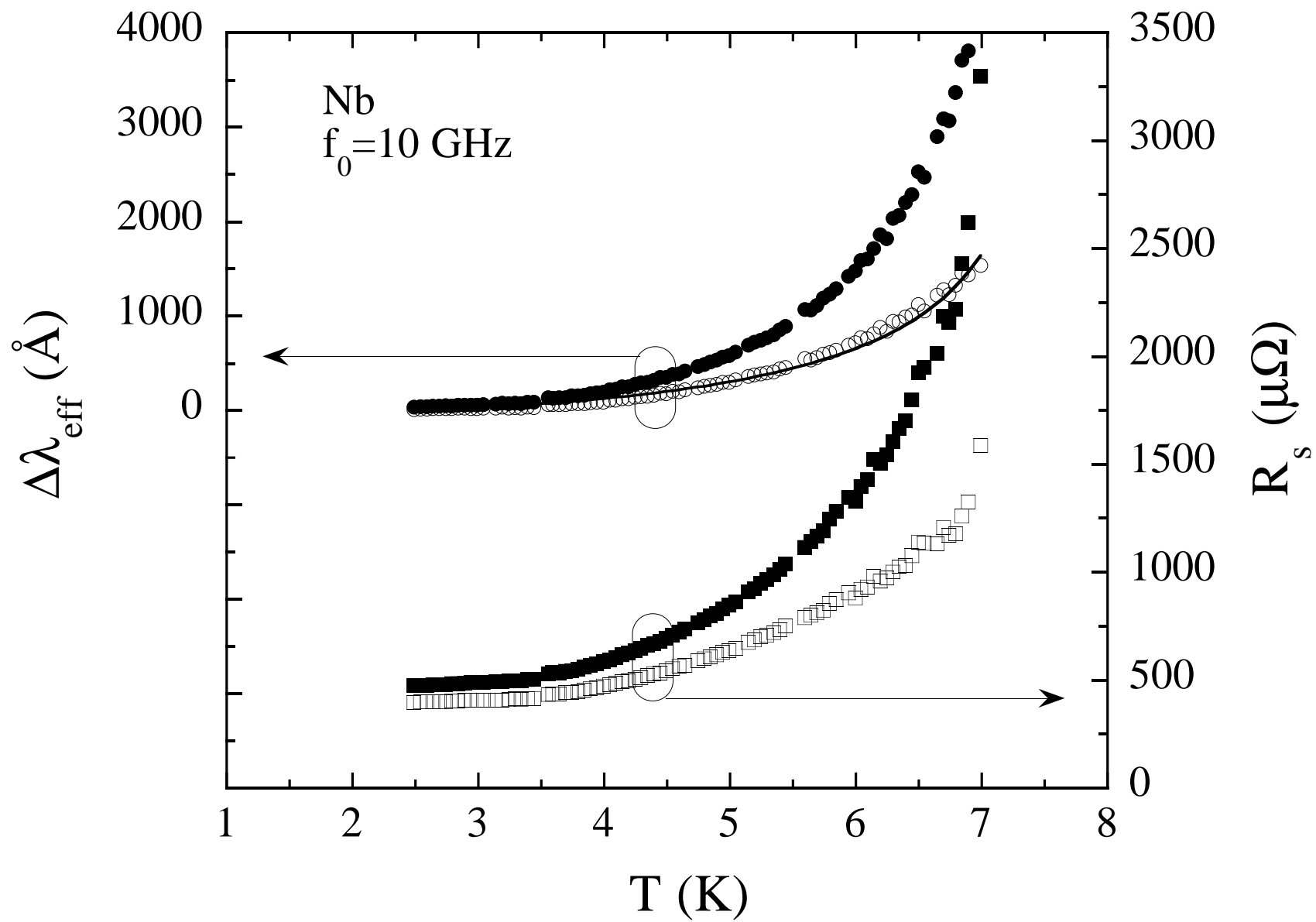


Fig. 4  
L. V. Mercaldo et al.

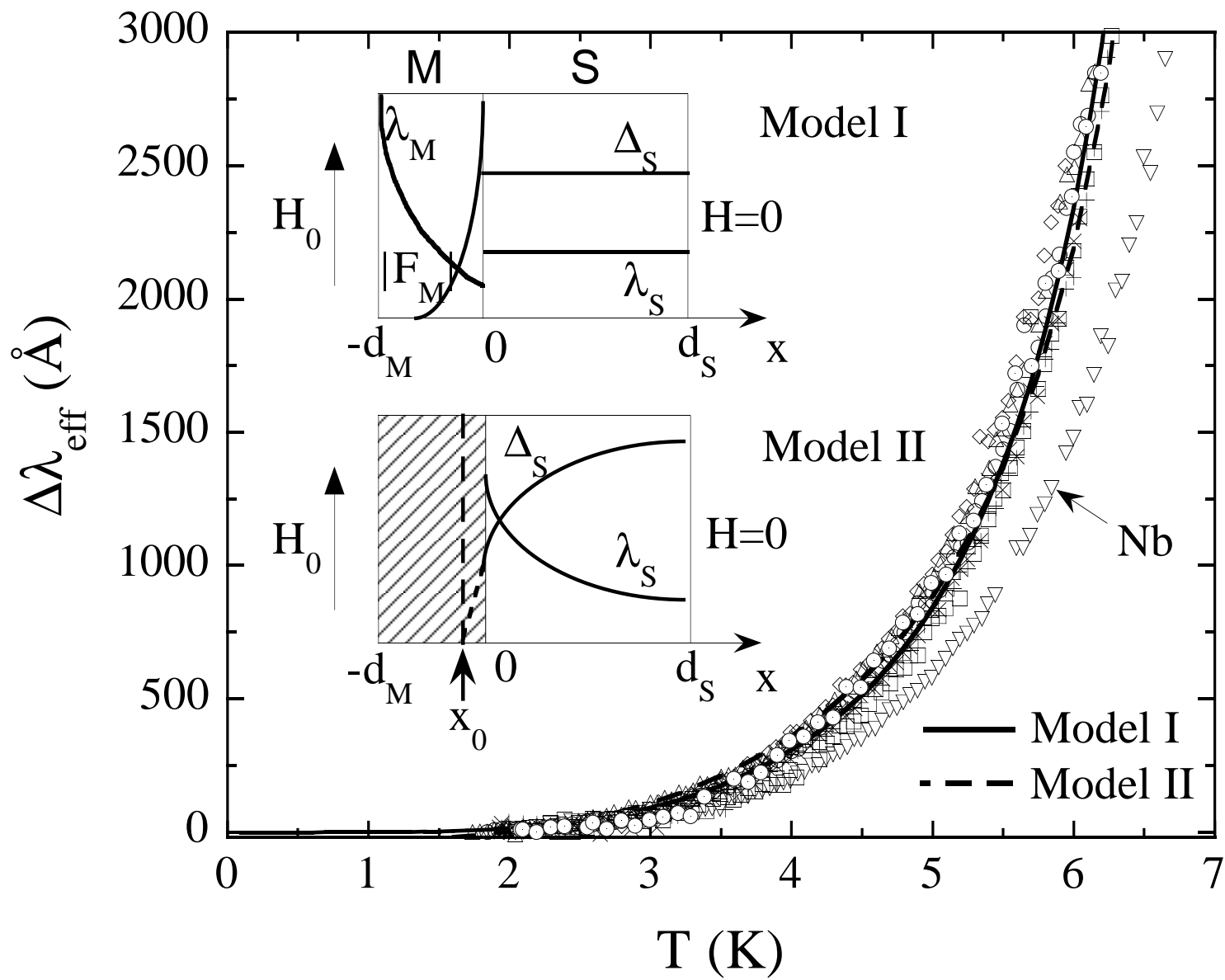


Fig. 5  
 L. V. Mercaldo et al.

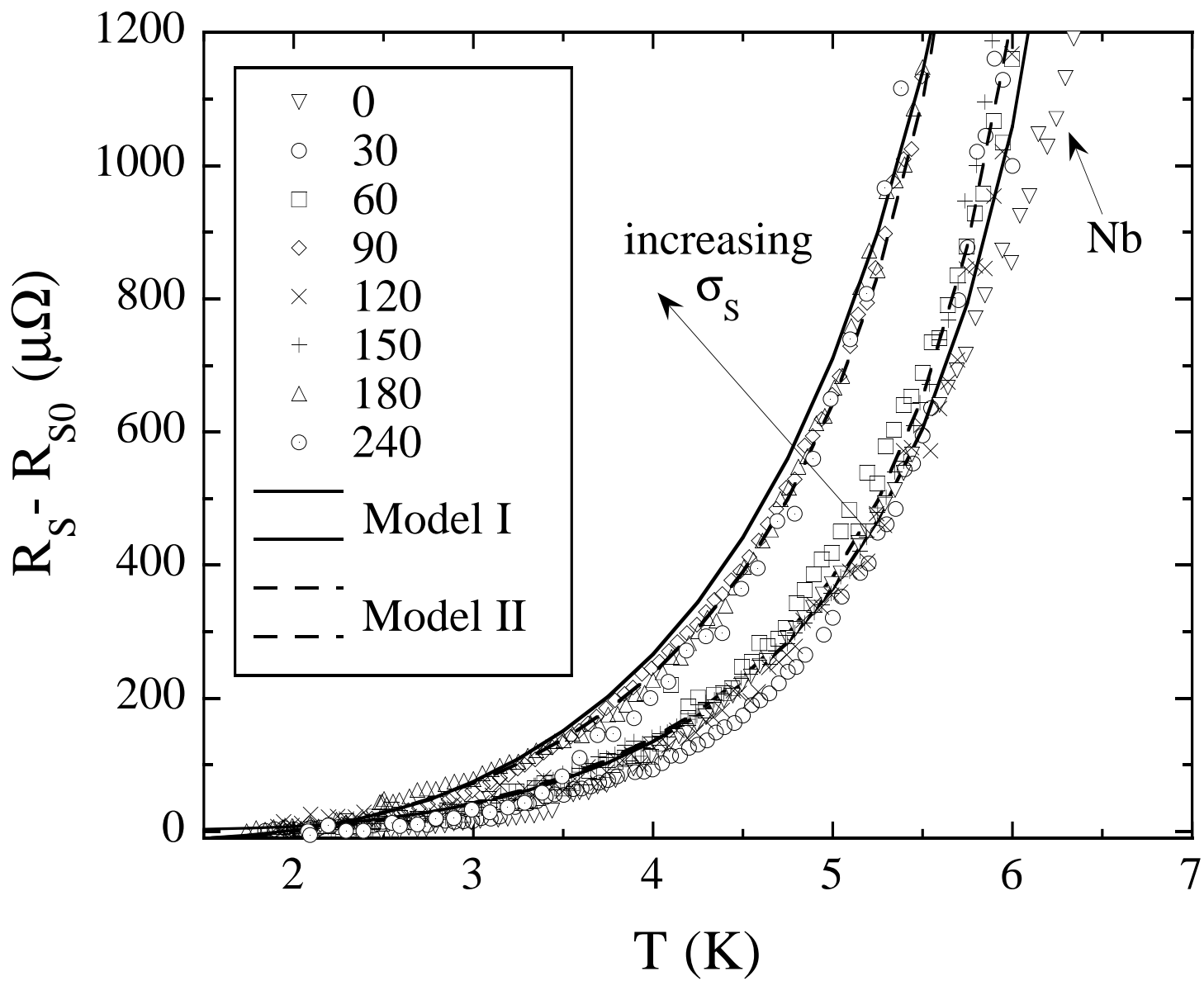


Fig. 6  
L. V. Mercaldo et al.